



# Effect of carbon nanotubes on the interface evolution and dielectric properties of polylactic acid/ethylene–vinyl acetate copolymer nanocomposites

Ping Wang<sup>1,2,3</sup> · Tao Song<sup>1,2,3</sup> · Hala M. Abo-Dief<sup>4</sup> · Jie Song<sup>1,2,3</sup> · Abdullah K. Alanazi<sup>4</sup> · Bingyu Fan<sup>1,2,3</sup> · Mina Huang<sup>5</sup> · Zhiping Lin<sup>6</sup> · Amal A. Altalhi<sup>4</sup> · Shang Gao<sup>1,2,3</sup> · Liyuan Yang<sup>1,2,3</sup> · Jin Liu<sup>1,2,3</sup> · Shaojie Feng<sup>1,2,3</sup> · Tian Cao<sup>1,2,3</sup>

Received: 5 April 2022 / Revised: 25 April 2022 / Accepted: 7 May 2022 / Published online: 7 June 2022  
© The Author(s), under exclusive licence to Springer Nature Switzerland AG 2022

## Abstract

The composites of polylactic acid/glycidyl methacrylate of grafted ethylene–vinyl acetate copolymer/ethylene–vinyl acetate copolymer/carbon nanotubes (PLA/EVA-*g*-GMA/EVA/CNTs) were prepared by melt-blended. The effects of CNTs on the interfacial morphological evolution and dielectric properties of the PLA/EVA-*g*-GMA/EVA composites were investigated. The introduction of CNTs reduced the reaction efficiency of epoxy groups in EVA-*g*-GMA with terminal hydroxyl and terminal carboxyl groups of the PLA, which resulted in a decrease in the mechanical properties of the materials slightly. In addition, the introduction of CNTs as a solid filler which limited the movement of PLA segment thus caused the PLA crystal to grow slowly, which reduced the crystallization ability of the PLA, but improved the thermal stability of the composite material. Most importantly, the introduction of CNTs obviously improved the dielectric properties of the composites. Only 1% CNTs need to be added, and the dielectric constant of composites was increased from 5.81 to 11.08; at the same time, the tensile strength and elongation at break can reach 42.7 MPa and 70.5%, respectively. The material has both electrical properties and good balance of stiffness and toughness. This work offers an innovative methodology for facilely and massively creating high-performance multi-component PLA composites which can expand the application of PLA-based biodegradable materials in micron storage capacitors, integrated circuits, and other electronic fields.

**Keywords** Polylactic acid · Carbon nanotubes · Dielectric properties · Blending · Composite materials

## 1 Introduction

Polymer materials are considered to be ideal carriers for the preparation of flexible dielectric materials due to their low dielectric loss, easy processing, and good flexibility [1–5]. However, the lower dielectric constant and higher dielectric loss of polymer materials limit their applications in electronic fields such as miniature storage capacitors and integrated circuits [6–8]. Currently, there are two methods for preparing polymer dielectric materials with high dielectric constant. One is to modify the polymer backbone by introducing high polar functional groups with weakly dipole-coupled or by introducing macromolecular structures into the polymer backbone to enhance the dielectric properties and energy storage capacity of the polymer dielectric by inhibiting dipole–dipole interactions [9–11]. In this approach, although the dielectric polymer with a higher dielectric constant and a higher energy storage capacity is obtained, the new type of

✉ Ping Wang  
anjzwp@ahjzu.edu.cn

<sup>1</sup> Anhui Province International Research Center On Advanced Building Materials, School of Materials and Chemical Engineering, Anhui Jianzhu University, Hefei 230601, China

<sup>2</sup> Anhui Province Key Laboratory of Advanced Building Materials, Anhui Jianzhu University, Hefei 230601, China

<sup>3</sup> National and Local Joint Engineering Research Center for Special Wire and Cable Branch Center of Anhui Jianzhu University, Anhui Jianzhu University, Hefei 230601, China

<sup>4</sup> Department of Chemistry, College of Science, Taif University, P.O. Box 11099, Taif 21944, Saudi Arabia

<sup>5</sup> College of Materials Science and Engineering, Taiyuan University of Science and Technology, Taiyuan 030024, China

<sup>6</sup> Department of Materials Science and Engineering, Taizhou University, Taizhou 318000, China

dielectric polymer prepared requires a complicated organic synthesis and manufacturing process, which is difficult to achieve large-scale manufacturing of polymers [11].

In comparison, the introduction of conductive nanoparticles into the polymer matrix by melt blending to prepare dielectric nanomaterials is a very promising method that not only combines the relatively high dielectric constant of conductive nanoparticles and breakdown strength but also combines the flexibility and ease of processing of polymer materials [12, 13]. For example, Yuan et al. prepared high dielectric constant polymer-based nanocomposites with a dielectric constant of 3800 by introducing carbon nanotubes (CNTs) into the PVDF matrix by melt blending [14]. Amelie et al. prepared polypropylene-CNTs nanocomposites with porous structures by melt blending and physical foaming [15]. This preparation method increased the dielectric constant of the nanocomposites by an order of magnitude.

However, in most studies on polymer dielectric composites, non-biodegradable petroleum-based polymers are used as substrates to prepare polymer dielectric composites [16–19]. This not only causes the waste of petroleum resources but also seriously threatens the ecological environment of human life [20, 21]. In this context, biodegradable polylactic acid (PLA) derived from renewable resources instead of traditional petroleum-based polymers as the preparation of composite materials with excellent dielectric properties has attracted widespread attention. For example, Giovanni et al. investigated the effect of carbonaceous particles such as CNTs and graphene nanosheets (GNPs) on the dielectric properties of PLA composites by filling them with PLA. They found that when 12 wt% CNTs were introduced, the relative dielectric constant of PLA composites reached  $5.35 \times 10^3$  [22]. Wu et al. prepared PLA/CNTs@TiO<sub>2</sub> nanocomposites with preferably dielectric properties by introducing CNTs@TiO<sub>2</sub> into PLA [23]. These studies indicate that the introduction of CNTs can improve the dielectric properties of PLA.

In addition, long-term studies have found that the percolation threshold in polymer matrix decreases with the increase of filler particle aspect ratio, especially for rod-like conductive nanoparticles, whose higher aspect ratio is the best filler for preparing dielectric nano-polymer materials [3, 24]. Therefore, CNTs fillers with high aspect ratio, high surface area, and unique electrical, thermal, and mechanical properties have received a lot of extensive attention in charge storage or capacitor applications [25–28]. In particular, blending CNTs with polymers is one of the main methods for preparing polymer dielectric materials [29, 30]. Among them, CNTs dispersed in the polymer matrix can act as the electrode of nanocapacitors, resulting in a significant increase in space charge polarization. Moreover, the high conductivity of CNTs increases the interfacial polarization between CNTs and the polymer interfacial layer. Its high specific surface area can improve the interface polarization

density [31–33]. Therefore, one-dimensional fillers such as CNTs are better suited for enhancing the dielectric properties of biodegradable polymer materials [22]. However, because of the complex dispersion behavior of CNTs in the polymer matrix and the limitation of inherent brittleness of PLA, it is difficult to prepare dielectric composites with high performance after blending CNTs. Therefore, while achieving excellent dielectric properties of PLA/CNTs composites, blending modification is usually required to toughen the PLA composites. Current studies have found that blending with polyester elastomers with better flexibility is one of the most efficient ways to enhance the toughness of PLA [34–37]. Among them, ethylene–vinyl acetate copolymer (EVA) can regulate its compatibility with PLA by controlling the content of VA in the molecular chain and improving the toughness of PLA substrate [38–41]. However, the effect of simply increasing VA content in EVA to improve interface compatibility between EVA and PLA has limited effect, and when inorganic filler is introduced into PLA/EVA blend system, the dispersion state of filler in the matrix is poor, and it is difficult to achieve high performance of PLA/EVA. Previous studies of our research group showed that glycidyl methacrylate (GMA) and its copolymer containing epoxy groups could improve the interface compatibility of PLA blends through the carboxy-terminated and hydroxy-terminated reactions between epoxy groups and PLA, and also regulate the dispersion of inorganic fillers such as CNTs in PLA matrix. The preparation of super-tough PLA composite was realized [30, 42, 43].

In this study, CNTs were introduced into PLA and EVA blends, and glycidyl methacrylate grafted ethylene–vinyl acetate copolymer (EVA-g-GMA) was used as the interfacial compatibilizer of PLA/EVA blends to enhance the interfacial compatibility between PLA and EVA, which could improve the toughness of PLA/EVA blends. The controllable dispersion of CNTs was induced and the dielectric properties of polylactic acid composites were improved. The effects of CNTs on PLA/EVA-g-GMA/EVA composites condensed structure, microstructure evolution, machining properties, mechanical properties, thermal stability, and dielectric properties were studied respectively, and the influence mechanism of CNTs on microstructure evolution and macroscopic properties was clarified.

## 2 Experimental section

### 2.1 Materials

Polylactic acid (PLA, 4032D) with a number average molecular weight of 120 kg/mol, a poly-dispersity index (PDI) of 1.78, was purchased from Nature works Co. Ltd., USA. Ethylene–vinyl acetate copolymer (EVA, 42–60, VA content: > 41 wt%) was

purchased from Arkema Co. Ltd., France. Glycidyl methacrylate grafted ethylene–vinyl acetate copolymer (EVA-*g*-GMA) with the grafted rate of 1.4~2.0% was obtained from Arkema Co. Ltd., France. Carbon nanotubes (CNTs) without any further treatment were obtained from Nanjing XFNANO Materials Tech Co. Ltd., China.

## 2.2 Sample preparation

The completely dried PLA, EVA, EVA-*g*-GMA, and CNTs were added to the torque rheometer (RM-200C) at 180 °C according to the ratio in Table 1. The torque change was observed during the blending process, and the blending was continued for 6 min after the torque was balanced. The samples were compressed by a hot-pressing machine (XH-406, Dongguan Xihua Machinery Technology Co. Ltd., China). The process parameters of temperature and pressure for hot-pressing machine were 180 °C and 10 MPa.

## 2.3 Characterization

The torque variation of PLA/EVA composites during the processing was recorded by the torque rheometer (RM-200C, Harp, China). Thermogravimetric analysis of the samples was tested on thermal analyzer equipment (TA-Q500, TA Instruments) at a heating rate of 10 °C/min and in a nitrogen atmosphere. The non-isothermal crystallization properties of PLA/EVA composites were investigated by a differential scanning calorimeter (TA-Q2000, TA Instruments). The mass of the sample was approximately 5–10 mg in an aluminum crucible. All samples were tested under the condition of a nitrogen purge rate of 50 mL/min. The first stage was the heating process, and all the samples were heated from 25 to 200 °C at a heating rate of 10 °C/min and held for 300 s to eliminate the thermal history. The second stage was the cooling process, and all the samples were then cooled down to –60 °C at a constant rate of 10 °C/min. The third stage was the second heating process, the sample was heated from –60 to 200 °C at a heating rate of 10 °C/min. The phase morphologies of PLA/EVA composites were observed by a tungsten filament scanning electron microscope (JSM-6490LV, Japan Electronics Manufacturing Co. Ltd.) and the dispersion states of CNTs in the PLA/EVA composites were investigated by a cold field emission

scanning electron microscope (SU8020, Japan Hitachi Company). All the samples were frozen in liquid nitrogen for 5 min and then brittle fractured. The phase morphologies in the blends of the cryofracture surface and the dispersion state of CNTs in the PLA/EVA composites were characterized at the condition of 15 kV and 5 kV accelerating voltage.

The mechanical properties of PLA/EVA composite materials were investigated by a microcomputer-controlled electronic universal testing machine (CMT4304, MTS Industrial Systems Co. Ltd.). The tensile specimens of a dumbbell shape were tested by a universal testing machine with a cross-head speed of 5 mm/min according to the ISO 527 standard.

The dielectric properties of the composite materials were tested by the E4980A LCR dielectric measuring instrument (Agilent Technologies Co. Ltd., USA). Dielectric test samples were molded with a plate vulcanizer to mold a square sample of 40 mm × 40 mm × 0.3 mm. Before the test, a layer of silver paste with a diameter of 10 mm was uniformly coated in the middle of the sample to form a silver electrode. The dielectric performance test was carried out at room temperature and the measurement was performed in the frequency range of 20 Hz to 2 MHz.

## 3 Results and discussion

### 3.1 Processing properties

The torque-time curves of PLA/EVA composites with different contents of CNTs are presented in Fig. 1. As we all know, the melt torque is an important parameter for evaluating the melt viscosity and the interaction between melt during polymer processing. As shown in Fig. 1, the final equilibrium torque of the PLA/EVA material was 8.3 N·m. The trend of the final equilibrium torque of the composite

**Table 1** Composition of the prepared PLA/EVA composites

Sample	PLA/g	EVA/g	EVA- <i>g</i> -GMA/g	CNTs/g
PLA/EVA	44.32	4.93	0.75	0
PLA/EVA/0.5CNTs	44.1	4.9	0.746	0.25
PLA/EVA/1.0CNTs	43.88	4.88	0.743	0.5
PLA/EVA/1.5CNTs	43.66	4.85	0.74	0.75

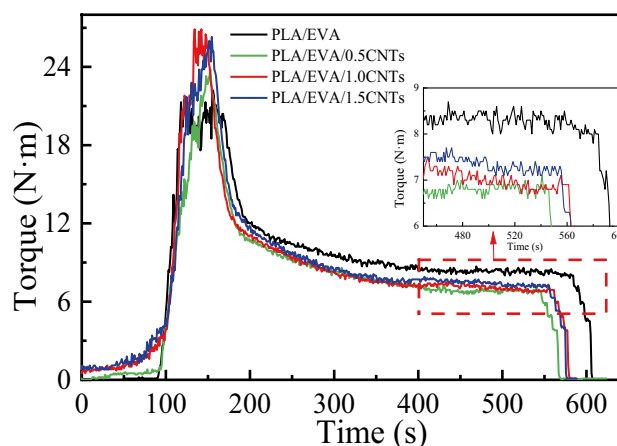


**Fig. 1** The torque versus time during the melting blending for PLA/EVA composites

material in Fig. 1 shows a decrease as the CNTs are incorporated. This is mainly due to the existence of CNTs that reduced the reaction probability between the epoxy group in EVA-*g*-GMA and the PLA terminal hydroxyl or terminal carboxyl group, which leads to a decrease in the degree of cross-linking, resulting in a decrease in the compatibility of PLA and EVA. As the content of CNTs increases, the equilibrium torque of the composites gradually increases, as illustrated in the enlarged view in Fig. 1. This is because CNTs are hard materials, and incorporating them into polymer materials will increase the viscosity of the system [44]. At the same time, the presence of CNTs can promote the physical crosslinking of the PLA/EVA blend system, resulting in an elevated system viscosity and increased torque.

## 3.2 Thermal property

### 3.2.1 Thermal stability

The effects of CNTs content on the thermal degradation of PLA/EVA composites were investigated by thermogravimetric analysis (TGA). The TGA and DTG curves for PLA/EVA/CNTs composites are shown in Fig. 2. The TGA data, including the initial decomposition temperature ( $T_{5\%}$ ), the temperature of maximum decomposition rate of PLA ( $T_{max\ PLA}$ ), and the temperature of maximum decomposition rate of EVA ( $T_{max\ EVA}$ ) of all PLA/EVA composites are presented in Table 2. All the samples underwent a two-step thermal decomposition behavior, corresponding to the thermal degradation of PLA and EVA chains, respectively. The weight loss within 300–380 °C is mainly contributed by the thermal decomposition of PLA, and part of the contribution of thermal weight loss comes from the removal of acetic acid in EVA, forming C=C double bonds along the polymer backbone. When the temperature exceeds 380 °C, the weight loss is mainly caused by the EVA main chain, breaking into various hydrocarbon volatilization [45]. It shows that PLA degrades earlier than EVA as shown in the enlarged view in Fig. 2a, indicating that PLA has poor thermal stability compared with EVA. Based on the results shown in Table 2, the PLA/EVA blend without CNTs has a thermal

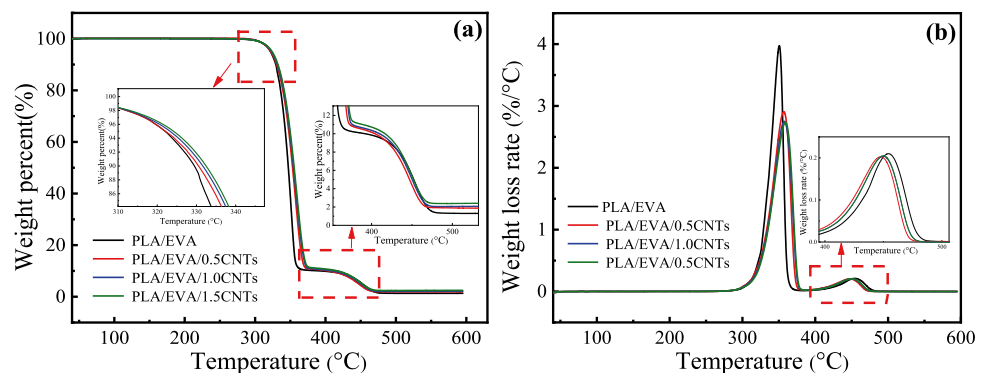
**Table 2** Thermal stability parameters of PLA/EVA composites

Sample	$T_{5\%}$ (°C)	$T_{max\ PLA}$ (°C)	$T_{max\ EVA}$ (°C)
PLA/EVA	321.9	350.5	454.5
PLA/EVA/0.5CNTs	322.1	356.8	447.8
PLA/EVA/1.0CNTs	323.3	357.5	450.1
PLA/EVA/1.5CNTs	324.2	359.1	450.1

decomposition temperature ( $T_{5\%}$ ) of only 321.9 °C at 5 wt% mass loss, which is the worst thermal stability. Compared with that of the PLA/EVA material, the thermal stability of the composites incorporated with nanofiller CNTs is further improved. In particular, the  $T_{5\%}$  of the PLA/EVA/CNTs composites was elevated, therefore the thermal stability of the PLA/EVA/CNTs composite was significantly improved. The above phenomenon shows that the introduction of CNTs improves the thermal stability of PLA/EVA composites. This increase in the initial thermal decomposition temperature was mainly due to the fact that CNTs prevent the movement of polymer segments and increase the difficulty of the arrangement of polymer segments [46].

The DTG curves (Fig. 2b) were obtained by temperature derivation of TG curves, and the effects of CNTs on the PLA and EVA phases were studied. The peak near 350 °C represents the decomposition of the PLA phase and the peak near 450 °C represents the break of the EVA backbone. With the increase of CNTs content, the peak value corresponding to the maximum decomposition rate gradually moves towards high temperature. By comparing with  $T_{max\ PLA}$  in the composites, it was found that the  $T_{max\ PLA}$  of PLA/EVA material without CNTs was the highest, and the  $T_{max\ PLA}$  decreased with the increase of CNTs content. This is due to the physical barrier effect of CNTs, and the homogeneous dispersion of CNTs will prevent the migration of the decomposition products in the composites, reduce the occurrence of autocatalytic degradation, and finally hinder the thermal degradation of PLA/EVA composites, which improve the thermal stability of the composite [47]. The thermal stability of EVA phase was decreased and the decomposition of EVA phase was

**Fig. 2** a TGA curves and b DTG curves of PLA/EVA composites under nitrogen



advanced by introducing CNTs into EVA phase as shown in the enlarged view in Fig. 2b.

### 3.2.2 Melting and crystalline behavior

The effect of CNTs on the melting and crystallization behavior of PLA/EVA composites was researched by DSC. The DSC curves of PLA/EVA/CNTs composites are presented in Fig. 3, and the crystallization kinetic parameters of PLA/EVA composites are summarized in Table S1. The DSC cooling curve for PLA and PLA/EVA composites in Fig. 3a is very smooth. The results show that the melt of PLA is more difficult to crystallize than the cold crystallization of PLA during heating up. However, due to the limited crystallization space of EVA, two indistinct restricted crystallization peaks appear at around 40 °C and 5 °C, respectively [48]. Meanwhile, with the increase of CNTs content, the crystallization peak of EVA moved to the direction of low temperature, and the crystallization enthalpy is also significantly reduced, which is because the addition of CNTs reduces the phase size of EVA, so that the restricted crystal of EVA is more obvious.

The second melting scan curves of PLA/EVA/CNTs composites are shown in Fig. 3b. The glass transition temperature ( $T_g$ ) of PLA/EVA blends without CNTs is 60.5 °C (Table S1). With the increase of CNTs content, the  $T_g$  of PLA is increased slightly, which is mainly caused by the restriction of the movement of PLA chain segments by CNTs. For PLA/EVA/CNTs composites, with the increase of CNTs content, the value of cold crystallization temperature ( $T_{cc}$ ) is decreased from 111.9 to 109.4 °C, while the value of crystallinity ( $\chi_c$ ) is also reduced. The decreased  $T_{cc}$  is due to the nucleation of CNTs. However, the crystallization at lower temperature will lead to the formation of some imperfect crystals, which in turn will act as the cross-links between the macromolecular chains; therefore, the chain mobility and the ability of further crystallization of the chain are further reduced, which leads to the decrease of the crystallinity of the composites.

The melt peaks and melting points of the PLA/EVA composites were observed, and all PLA/EVA composites showed a typical double melt-peak, which is because of the melting-recrystallization-remelting processes of the PLA component [49]. Specifically, the imperfect crystal caused by cold crystallization partially melts during heating, and the unmelted part can be acted as the nucleation site of PLA, which promotes the recrystallization of PLA. So, the crystals formed during recrystallization has a thicker wafer and a perfect crystal structure, which require higher temperatures to melt, resulting in a double melting peak. In addition, the melt peak at low temperatures is observed to gradually decrease as the CNTs content increases, due to the entanglement of PLA chains caused by CNTs and the incomplete crystals formed during cold crystallization which reduces the chain migration rate of PLA. This causes the incomplete crystal growth formed during the cold crystallization to slowly and lead to the decrease of melting peaks.

### 3.3 Morphological analysis

The morphologies of the cryofracture surfaces of the PLA/EVA composites were observed by SEM, and the evolution of the phase morphology of the PLA/EVA composites by the content of CNTs was studied. Figure 4 shows the micrographs of the cryofracture surfaces of the PLA/EVA/CNTs composites with 0, 0.5, 1, and 1.5 wt% CNTs. According to the micrographs, the PLA/EVA blend without CNTs exhibits a typical sea-island structure. PLA serves as a continuous phase, and EVA as the dispersed phase presents a regular spherical shape of different sizes, which closely adheres to PLA. This indicates a good interfacial adhesion from PLA and EVA, which might be related to the lower viscosity of the PLA phase. The lower viscosity increases the possibility and ease of aggregation of EVA in PLA-rich samples [50]. The particle size of EVA dispersed phase is gradually decreased significantly with the addition of CNTs and gradually deformed from a regular spherical shape to an irregular

**Fig. 3** DSC curves of PLA/EVA composites; **a** cooling curve, and **b** heating curve

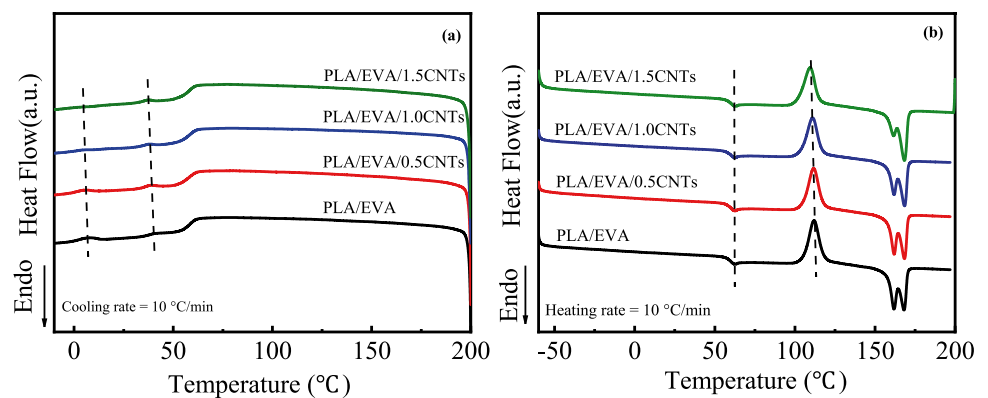
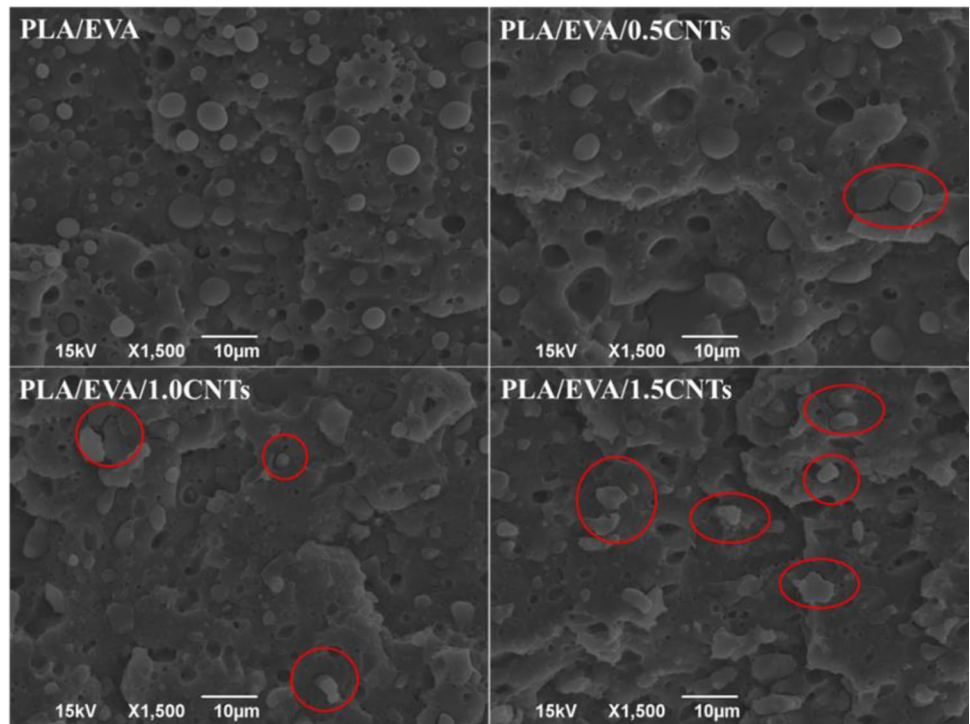


**Fig. 4** SEM images of the cryo-fracture surfaces of the PLA/EVA composites



shape. This phenomenon might be due to the increase in the viscosity of the system caused by the introduction of CNTs, and the change in the viscosity ratio of the blend components is also one of the reasons for the change in the phase morphology of the composites. The EVA phase and PLA phase of PLA/EVA composites have gaps with the increase of CNTs content. This is because the introduction of CNTs reduces the reaction efficiency of the epoxy group in the compatibilizer EVA-g-GMA with PLA, so the interfacial adhesion between PLA phase and EVA phase is reduced, which results in a reduction in the mechanical properties of composites.

### 3.4 Mechanical properties

Figure 5 shows the mechanical properties of PLA/EVA/CNTs composites with different contents of CNTs. The tensile

stress-strain curves of the PLA/EVA composites are shown in Fig. 5a. The tensile strength and the elongation at break of the PLA/EVA/CNTs composites are summarized in Fig. 5b. The PLA/EVA blends material demonstrates the highest mechanical properties, and its tensile strength and elongation at break reach 53.4 MPa and 255.8%, respectively. The mechanical properties of the PLA/EVA composites are degraded gradually with the addition of CNTs. Although both the tensile strength and elongation at break are decreased after the introduction of CNTs, PLA/EVA/CNTs composites at different scales have a good rigid balance. In order to better describe the effect mechanism of CNTs on the mechanical properties of PLA/EVA/CNTs composites, Fig. 6 shows the SEM images of the tensile fractured surface of PLA/EVA composites. All composites show the fibrous tensile fracture surfaces of typical toughness fractures, which indicates that the composites have a good toughness when CNTs are added.

**Fig. 5** a Stress–strain curve and b mechanical parameters of PLA/EVA composites

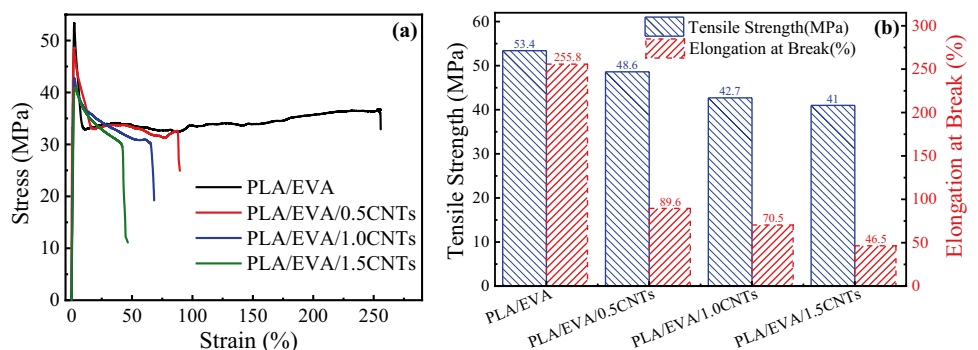
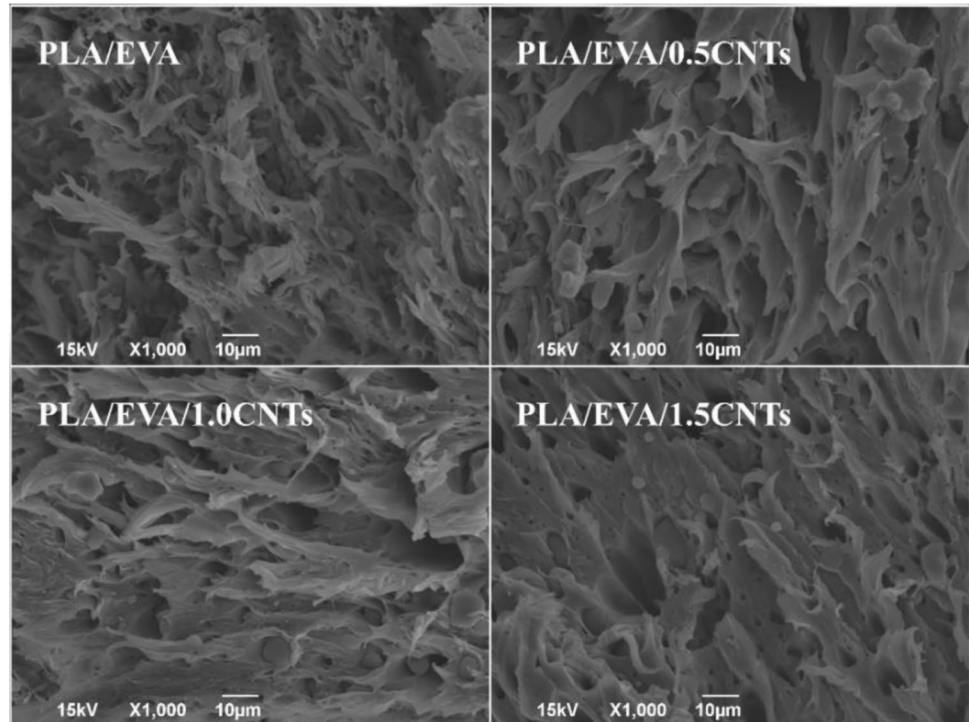


**Fig. 6** SEM micrographs for the tensile fractured surfaces of PLA/EVA composite



### 3.5 Dielectric properties

Figure 7 shows the relationship between (a) dielectric constant ( $\epsilon'$ ) and (b) dielectric loss tangent ( $\tan \delta$ ) of PLA/EVA composites with different contents of CNTs at 30 °C (the composite material of PLA/EVA/1.5CNTs is not shown in the figure due to the high  $\tan \delta$ ). After the introduction of CNTs, the  $\epsilon'$  of the composites is increased significantly, especially when 1% CNTs is introduced, the  $\epsilon'$  of PLA/EVA/1.0CNTs composites is increased to 11.08, which is twice that of PLA/

EVA blends. As the content of CNTs increases, the  $\epsilon'$  of PLA/EVA composites is gradually increased. The reason for this phenomenon may be that in the composite material, the adjacent CNTs are used as the electrode and the polymer between the adjacent carbon tubes is used as the dielectric to assemble the micro capacitor, greatly increase the local electric field intensity and effectively increase the interface polarization, which result to the increase of  $\epsilon'$  [51].

In Fig. 7b, the variation of  $\tan \delta$  is the same as  $\epsilon'$ , and the lowest  $\tan \delta$  of PLA/EVA blends is 0.009 at 100 Hz. After

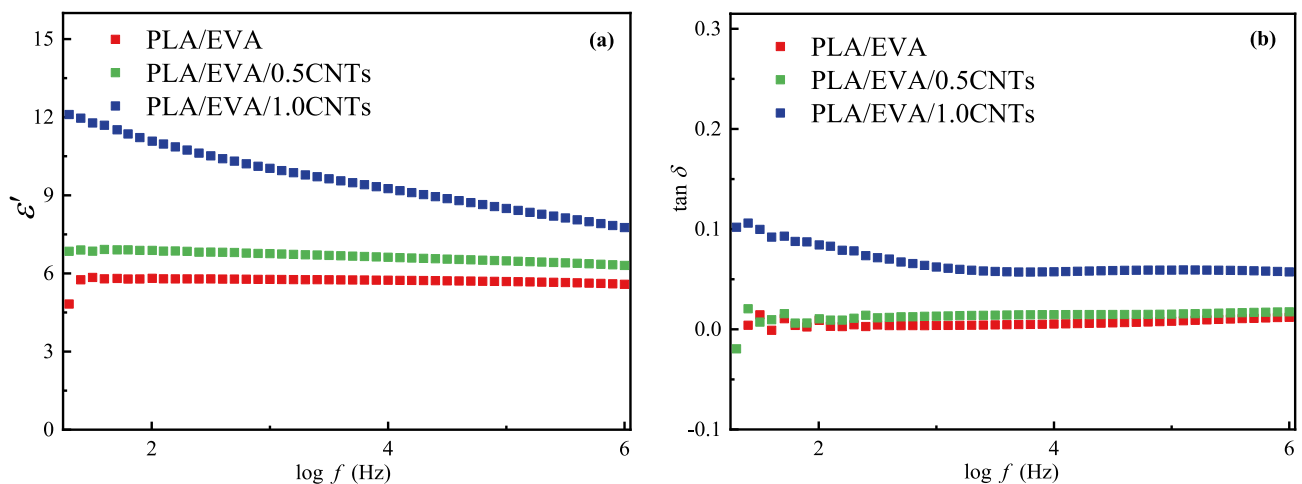


**Fig. 7** Frequency dependence of **a**  $\epsilon'$  and **b**  $\tan \delta$  for the PLA/EVA composites

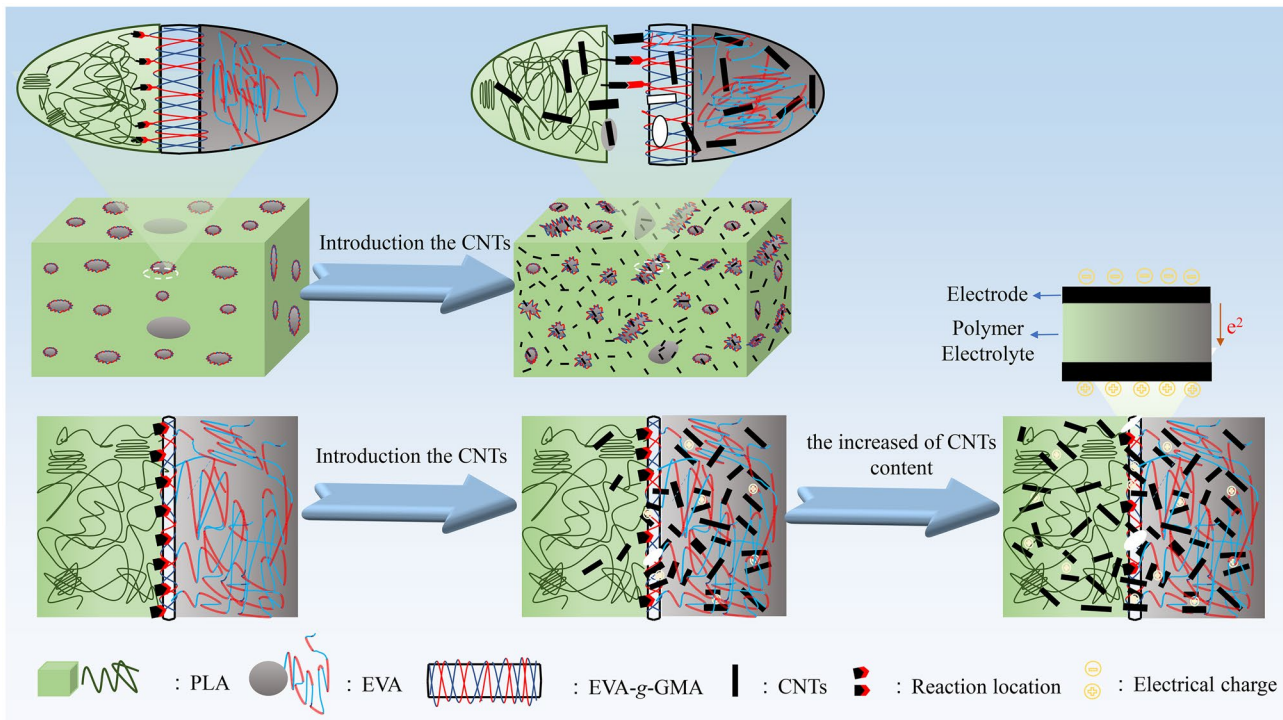


**Fig. 8** Schematic illustration of the mechanisms of microstructure evolution for PLA/EVA/CNTs composites

the introduction of CNTs, the  $\tan \delta$  of PLA/EVA/CNTs composites is significantly increased, especially when the content of CNTs is 1 wt%, the  $\tan \delta$  of PLA/EVA/1.0CNTs is 0.084 at 100 Hz. As we all know, the interface bonding force between PLA and EVA is reduced with the introduction of CNTs (Fig. 4), which causes an increase in the interface defects and leakage current, and ultimately results in an increase in  $\tan \delta$  [52]. Combining with the mechanical properties, it can be found that PLA/EVA/1.0CNTs composites have high dielectric properties, but still maintain better mechanical properties than PLA and have potential application value in dielectric materials.

### 3.6 Interface evolution mechanism

Figure 8 shows the schematic illustration of the mechanisms of microstructure evolution for PLA/EVA/CNTs composites. In the PLA/EVA blends without CNTs, the EVA-g-GMA is wrapped on the surface of the EVA phase, and the terminal hydroxyl group of the PLA is chemically reacted between the epoxy group of the EVA-g-GMA, resulting in a micro-crosslinking structure, which improved the interfacial interaction between PLA phase and EVA phase and enhanced the interface bonding force. With the introduction of CNTs, the structure and properties of PLA/EVA composites have changed significantly. The evolution behavior of CNTs on the microstructure of PLA/EVA

composites is related to the distribution of CNTs in PLA phase and EVA phase. Due to the better affinity between CNTs and EVA, CNTs tend to migrate to the EVA phase first. As shown in Fig. 4, the particle size of EVA dispersed phase was gradually decreased with the addition of CNTs and gradually deformed from a regular spherical shape to an irregular shape, which indicated that CNTs affected the interface morphology of EVA. At the same time, the gap between EVA phase and PLA phase appeared in PLA/EVA composite material with the increased of CNTs content, because of the introduction of CNTs reduced the reaction efficiency of the epoxy group in the EVA-g-GMA with PLA, and decreased the interface adhesion between PLA phase and EVA phase, which resulted in the deterioration of material performance. Also, as shown in Fig. 6 with the introduction of CNTs, the fibers in the tensile section gradually got shorter and coarser, and a large number of undeformed EVA phases appeared at the fiber bottom, and the degree of interface peeling increased. Therefore, the CNTs preferentially migrated to the EVA phase with the introduction of CNTs. As the content of CNTs increased and the effected of shear force in the blending process, some CNTs migrated to the phase interface between PLA and EVA, while reduced the EVA-g-GMA interface reaction efficiency, but improved the interface polarization degree of PLA and EVA, and the dielectric properties of PLA/EVA composites were improved [53, 54].



## 4 Conclusions

The CNTs were introduced into the PLA/EVA blend system by the melt-blended, and the composites with high dielectric properties and excellent stiffness toughness balance were prepared. The effects of CNTs on the interfacial structure evolution behavior and performance of the PLA/EVA/CNTs nanocomposites were investigated. CNTs improved the thermal stability of the PLA/EVA composites and reduced the crystallization capability of the PLA. When the CNTs content reached 1.5 wt%, the thermal decomposition temperature of PLA was increased from 350.5 to 359.1 °C, and the crystallinity was decreased from 3.1 to 1.3%. The presence of CNTs reduced the probability of reaction between the epoxy groups in EVA-g-GMA and the terminal hydroxyl or end carboxy group in PLA, while the presence of CNTs led to an increase in interface defects, so that the mechanical properties of the material were decreased, but all proportions of PLA/EVA composites had a good balance of rigidity and toughness. In particular, after the introduction of CNTs, the polarization degree of PLA phase and EVA phase was effectively improved, and the dielectric constant of PLA/EVA composites was significantly improved. Especially, when the content of CNTs was 1 wt%, the dielectric constant was increased to 11.08, the tensile strength of the material was 42.7 MPa, and the elongation at break was maintained at 70.5%, which can be used to manufacture key components of electronic and electrical equipment such as supercapacitors and polymer batteries.

**Supplementary information** The online version contains supplementary material available at <https://doi.org/10.1007/s42114-022-00489-0>.

**Acknowledgements** This research was supported by the National Natural Science Foundation of China (No. 51903002), Major science and technology projects of Anhui Province (202103a05020031, 201903a05020027), Anhui Jianzhu University PhD Startup Fund (2019QDZ22) and University Collaborative Innovation Project of Anhui province (GXXT-2019-017), Hefei Key Technology Major R&D Projects (No. J2019G19), Wuhu Key Technology Major R&D Projects (No. 2020yf14), Research Fund for Postdoctoral Researchers in Anhui Province (2020B413), Taif University Researchers Supporting Project number (TURSP-2020/243).

## Declarations

**Conflict of interest** The authors declare no competing interests.

## References

- Dang ZM, Yuan JK, Zha JW, Zhou T, Li ST, Hu GH (2012) Fundamentals, processes and applications of high-permittivity polymer-matrix composites. *Prog Mater Sci* 57(4):660–723. <https://doi.org/10.1016/j.pmatsci.2011.08.001>
- Su Y, Zhou M, Sui G, Lan J, Zhang H, Yang X (2020) Polyvinyl butyral composites containing halloysite nanotubes/reduced graphene oxide with high dielectric constant and low loss. *Chem Eng J* 394:124910. <https://doi.org/10.1016/j.cej.2020.124910>
- Yuan JK, Yao SH (2016) Dielectric constant of polymer composites and the routes to high-k or low-k nanocomposite materials. *Polymer Nanocomposites* 1:3–28. <https://doi.org/10.1007/978-3-319-28238-1>
- Shen Y, Zhang X, Li M, Lin Y, Nan CW (2017) Polymer nanocomposite dielectrics for electrical energy storage. *Natl Sci Rev* 4(1):23–25. <https://doi.org/10.1093/nsr/nww066>
- Yu J, Zhang YM, Guo QW, Hou H, Ma Y, Zhao YH (2022) Effect of pressure on anisotropy in elasticity, sound velocity, and thermal conductivity of vanadium borides. *Adv Compos Hybrid Mater* 1–9. <https://doi.org/10.1007/s42114-021-00403-0>
- Shi L, Yang R, Lu S, Jia K, Xiao C, Lu T, Wang TJ, Wei W, Tan H (2018) Dielectric gels with ultra-high dielectric constant, low elastic modulus, and excellent transparency. *NPG Asia Mater* 10(8):821–826. <https://doi.org/10.1038/s41427-018-0077-7>
- Wu S, Li WP, Lin MR, Burlingame Q, Chen Q, Payzant A, Xiao K, Zhang QM (2013) Aromatic polythiourea dielectrics with ultrahigh breakdown field strength, low dielectric loss, and high electric energy density. *Adv Mater* 25(12):1734–1738. <https://doi.org/10.1002/adma.201204072>
- Su Y, Ren Y, Chen GX, Li Q (2016) Synthesis of high-k and low dielectric loss polymeric composites from crosslinked divinylbenzene coated carbon nanotubes. *Polymer* 100:179–187. <https://doi.org/10.1016/j.polymer.2016.08.043>
- Qiao Y, Islam MS, Han K, Leonhardt E, Zhang JY, Wang Q, Ploehn HJ, Tang CB (2013) Polymers containing highly polarizable conjugated side chains as high-performance all-organic nanodielectric materials. *Adv Func Mater* 23(45):5638–5646. <https://doi.org/10.1002/adfm.201300736>
- Zhang M, Zhang L, Zhu M, Wang YG, Li NW, Zhang ZJ, Chen Q, An LN, Lin YH, Nang CW (2016) Controlled functionalization of poly (4-methyl-1-pentene) films for high energy storage applications. *J Mater Chem A* 4(13):4797–4807. <https://doi.org/10.1039/C5TA09949H>
- Qiao Y, Yin X, Zhu T, Li H, Tang C (2018) Dielectric polymers with novel chemistry, compositions and architectures. *Prog Polym Sci* 80:153–162. <https://doi.org/10.1016/j.progpolymsci.2018.01.003>
- Zhao ZY, Zhao RX, Bai PK, Du WB, Guan RG, Tie D, Naik N, Huang MN, Guo ZH (2022) AZ91 alloy nanocomposites reinforced with Mg-coated graphene: phases distribution, interfacial microstructure, and property analysis. *J Alloy Compd* 902:163484. <https://doi.org/10.1016/j.jallcom.2021.163484>
- Zhao YL, Liu F, Zhu KJ, Maganti S, Zhao ZY, Bai PK (2022) Three-dimensional printing of the copper sulfate hybrid composites for supercapacitor electrodes with ultra-high areal and volumetric capacitances. *Adv Compos Hybrid Mater* 1–11. <https://doi.org/10.1007/s42114-022-00430-5>
- Yuan JK, Yao SH, Dang ZM, Sylvestre A, Genestoux M, Bai J (2011) Giant dielectric permittivity nanocomposites: realizing true potential of pristine carbon nanotubes in polyvinylidene fluoride matrix through an enhanced interfacial interaction. *J Phys Chem C* 115(13):5515–5521. <https://doi.org/10.1021/jp1117163>
- Ameli A, Wang S, Kazemi Y, Park CB, Pötschke P (2015) A facile method to increase the charge storage capability of polymer nanocomposites. *Nano Energy* 15:54–65. <https://doi.org/10.1016/j.nanoen.2015.04.004>
- Uyor UO, Popoola AP, Popoola O, Aigbodon VS (2018) Energy storage and loss capacity of graphene-reinforced poly (vinylidene fluoride) nanocomposites from electrical and dielectric properties perspective: a review. *Adv Polym Technol* 37(8):2838–2858. <https://doi.org/10.1002/adv.21956>

17. Alkan Ü, Kılıç M, Karabul Y, Çağlar M, İçelli O, Güven Özdemir Z (2018) X-ray irradiated LDPE/PP blends with high mechanical and dielectric performance. *J Appl Polym Sci* 135(31):46571. <https://doi.org/10.1002/app.46571>
18. Chi X, Liu W, Li S, Zhang X (2019) The effect of humidity on dielectric properties of PP-based nano-dielectric. *Materials* 12(9):1378. <https://doi.org/10.3390/ma12091378>
19. Sun J, Mu Q, Kimura H, Murugadoss V, He M, Du W, Hou C (2022) Oxidative degradation of phenols and substituted phenols in the water and atmosphere: a review. *Adv Compos Hybrid Mater* 1–14. <https://doi.org/10.1007/s42114-022-00435-0>
20. Yu Z, Yan Z, Zhang F et al (2022) Waterborne acrylic resin co-modified by itaconic acid and  $\gamma$ -methacryloxypropyl triisopropoxidesilane for improved mechanical properties, thermal stability, and corrosion resistance. *Prog Org Coat* 168:106875. <https://doi.org/10.1016/j.porgcoat.2022.106875>
21. Si YY, Li JN, Cui B, Tang DJ, Yang L, Murugadoss V, Maganti S, Huang MN, Guo ZH (2022) Janus phenol–formaldehyde resin and periodic mesoporous organic silica nanoadsorbent for the removal of heavy metal ions and organic dyes from polluted water. *Adv Compos Hybrid Mater* 1–16. <https://doi.org/10.1007/s42114-022-00446-x>
22. Spinelli G, Kotsilkova R, Ivanov E, Georgiev V, Ivanova R, Naddeo C, Romano V (2020) Dielectric spectroscopy and thermal properties of poly (lactic) acid reinforced with carbon-based particles: experimental study and design theory. *Polymers* 12(10):2414. <https://doi.org/10.3390/polym12102414>
23. Wu W, Liu T, Zhang D et al (2019) Significantly improved dielectric properties of polylactide nanocomposites via TiO<sub>2</sub> decorated carbon nanotubes. *Compos A Appl Sci Manuf* 127:105650. <https://doi.org/10.1016/j.compositesa.2019.105650>
24. An L, Boggs SA, Calame JP (2008) Energy storage in polymer films with high dielectric constant fillers. *IEEE Electr Insul Mag* 24(3):5–10. <https://doi.org/10.1109/MEI.2008.4591430>
25. Dang ZM, Wang L, Yin YI, Zhang Q, Lei QQ (2007) Giant dielectric permittivities in functionalized carbon-nanotube/electroactive-polymer nanocomposites. *Adv Mater* 19(6):852–857. <https://doi.org/10.1002/adma.200600703>
26. Ameli A, Nofar M, Park CB, Pötschke P, Rizvi G (2014) Polypropylene/carbon nanotube nano/microcellular structures with high dielectric permittivity, low dielectric loss, and low percolation threshold. *Carbon* 71:206–217. <https://doi.org/10.1016/j.carbon.2014.01.031>
27. Ma Y, Xie XB, Yang WY, Yu ZP, Sun XQ, Zhang YP, Yang XY, Kimura H, Hou CX, Guo ZH, Du W (2021) Recent advances in transition metal oxides with different dimensions as electrodes for high-performance supercapacitors. *Adv Compos Hybrid Mater* 4(4):906–924. <https://doi.org/10.1007/s42114-021-00358-2>
28. Gao SL, Zhao XH, Fu Q, Zhang TC, Zhu J, Hou FH, Ni J, Zhu CJ, Li TT, Wang YL, Murugadoss V, Mersal GAM, Ibrahim MM, El-Bahy ZM, Huang MN, Guo ZH (2022) Highly transmitted silver nanowires-SWCNTs conductive flexible film by nested density structure and aluminum-doped zinc oxide capping layer for flexible amorphous silicon solar cells. *J Mater Sci Technol*. <https://doi.org/10.1016/j.jmst.2022.03.012>
29. Dang ZM, Zheng MS, Zha JW (2016) 1D/2D carbon nanomaterial-polymer dielectric composites with high permittivity for power energy storage applications. *Small* 12(13):1688–1701. <https://doi.org/10.1002/sml.201503193>
30. Wang P, Zhou YY, Hu XH, Wang F, Chen JL, Xu P, Ding YS (2020) Improved mechanical and dielectric properties of PLA/EMA-GMA nanocomposites based on ionic liquids and MWCNTs. *Compos Sci Technol* 200:108347. <https://doi.org/10.1016/j.compscitech.2020.108347>
31. Kim JY, Kim T, Suk JW, Chou H, Jang JH, Lee JH, Kholmanov IN, Akinwande DJ, Ruoff RS (2014) Enhanced dielectric performance in polymer composite films with carbon nanotube-reduced graphene oxide hybrid filler. *Small* 10(16):3405–3411. <https://doi.org/10.1002/sml.201400363>
32. Jiang MJ, Dang ZM, Bozlar M, Miomandre F, Bai J (2009) Broad-frequency dielectric behaviors in multiwalled carbon nanotube/rubber nanocomposites. *J Appl Phys* 106(8):084902. <https://doi.org/10.1063/1.3238306>
33. Wu N, Zhao BB, Liu JY, Li YL, Chen YB, Chen L, Wang M, Guo ZH (2021) MOF-derived porous hollow Ni/C composites with optimized impedance matching as lightweight microwave absorption materials. *Adv Compos Hybrid Mater* 4(3):707–715. <https://doi.org/10.1007/s42114-021-00307-z>
34. Luyt AS, Gamsi S (2016) Influence of blending and blend morphology on the thermal properties and crystallization behaviour of PLA and PCL in PLA/PCL blends. *J Mater Sci* 51(9):4670–4681. <https://doi.org/10.1007/s10853-016-9784-z>
35. Messin T, Marais S, Follain N, Guinault A, Gaucher V, Delpouve N, Sollogoub C (2020) Biodegradable PLA/PBS multilayer membrane with enhanced barrier performances. *J Membr Sci* 598:117777. <https://doi.org/10.1016/j.memsci.2019.117777>
36. Xia M, Shi K, Zhou M, Shen Y, Wang T (2019) Effects of chain extender and uniaxial stretching on the properties of PLA/PPC/mica composites. *Polym Adv Technol* 30(9):2436–2446. <https://doi.org/10.1002/pat.4691>
37. Sangeetha VH, Valapa RB, Nayak SK, Varghese TO (2018) Investigation on the influence of EVA content on the mechanical and thermal characteristics of poly (lactic acid) blends. *J Polym Environ* 26(1):1–14. <https://doi.org/10.1007/s10924-016-0906-0>
38. Ouyang L, Huang W, Huang M, Qiu B (2022) Polyaniline improves granulation and stability of aerobic granular sludge. *Adv Compos Hybrid Mater* 1–11. <https://doi.org/10.1007/s42114-022-00450-1>
39. Ma P, Xu P, Zhai Y, Dong W, Zhang Y, Chen M (2015) Biobased poly (lactide)/ethylene-co-vinyl acetate thermoplastic vulcanizates: morphology evolution, superior properties, and partial degradability. *ACS Sustain Chem Eng* 3(9):2211–2219. <https://doi.org/10.1021/acssuschemeng.5b00462>
40. Li Y, Liu L, Shi Y, Xiang F, Huang T, Wang Y, Zhou Z (2011) Morphology, rheological, crystallization behavior, and mechanical properties of poly (l-lactide)/ethylene-co-vinyl acetate blends with different VA contents. *J Appl Polym Sci* 121(5):2688–2698. <https://doi.org/10.1002/app.33581>
41. Ma P, Hristova-Bogaerds DG, Goossens JGP, Spoelstra AB, Zhang Y, Lemstra PJ (2012) Toughening of poly (lactic acid) by ethylene-co-vinyl acetate copolymer with different vinyl acetate contents. *Eur Polym J* 48(1):146–154. <https://doi.org/10.1016/j.eurpolymj.2011.10.015>
42. Wang X, Mi J, Wang J, Zhou H, Wang X (2018) Multiple actions of poly (ethylene octene) grafted with glycidyl methacrylate on the performance of poly (lactic acid). *RSC Adv* 8(60):34418–34427. <https://doi.org/10.1039/C8RA07510G>
43. Paran SMR, Naderi G, Babakhani A (2018) An experimental study of the effect of CNTs on the mechanical properties of CNTs/NR/EPDM nanocomposite. *Polym Compos* 39(11):4071–4079. <https://doi.org/10.1002/pc.24467>
44. Jing XY, Li YC, Zhu JH, Chang, L Maganti S, Naik N, Xu BB, Murugadoss M, Huang M, Guo ZH (2022) Improving thermal conductivity of polyethylene/polypropylene by styrene-ethylene-propylene-styrene wrapping hexagonal boron nitride at the phase interface. *Adv Compos Hybrid Mater* 1–10. <https://doi.org/10.1007/s42114-022-00438-x>
45. Chaiwutthinan P, Chaujuljit S, Thipkham N, Kowalski CP, Boonmahitthisud A (2019) Poly (lactic acid)/ethylene vinyl acetate copolymer blend composites with wood flour and wollastonite: physical properties, morphology, and biodegradability. *J Vinyl Add Tech* 25(4):313–327. <https://doi.org/10.1002/vnl.21697>

46. Zhou Y, Lei L, Yang B, Li J, Ren J (2018) Preparation and characterization of polylactic acid (PLA) carbon nanotube nanocomposites. *Polym Testing* 68:34–38. <https://doi.org/10.1016/j.polymertesting.2018.03.044>
47. Mat Desa MSZ, Hassan A, Arsad A, Arjmandi R, Mohammad NNB (2016) Influence of rubber content on mechanical, thermal, and morphological behavior of natural rubber toughened poly (lactic acid)–multiwalled carbon nanotube nanocomposites. *J Appl Polym Sci* 133(48). <https://doi.org/10.1002/app.44344>
48. Xie Q, Bao J, Shan G, Bao Y, Pan P (2019) Fractional crystallization kinetics and formation of metastable  $\beta$ -form homocrystals in poly (l-lactic acid)/poly (d-lactic acid) racemic blends induced by previously formed stereocomplexes. *Macromolecules* 52(12):4655–4665. <https://doi.org/10.1021/acs.macromol.9b00644>
49. Behera K, Sivanjineyulu V, Chang YH, Chiu FC (2018) Thermal properties, phase morphology and stability of biodegradable PLA/PBSL/HAp composites. *Polym Degrad Stab* 154:248–260. <https://doi.org/10.1016/j.polymdegradstab.2018.06.010>
50. Aghjeh MR, Asadi V, Mehdijabbar P, Khonakdar HA, Jafari SH (2016) Application of linear rheology in determination of nanoclay localization in PLA/EVA/Clay nanocomposites: correlation with microstructure and thermal properties. *Compos B Eng* 86:273–284. <https://doi.org/10.1016/j.compositesb.2015.09.064>
51. Aigbodion VS (2021) Explicit microstructure and electrical conductivity of epoxy/carbon nanotube and green silver nanoparticle enhanced hybrid dielectric composites. *Nanocomposites* 7(1):35–43. <https://doi.org/10.1080/20550324.2020.1868690>
52. Guo N, DiBenedetto SA, Tewari P, Lanagan MT, Ratner MA, Marks TJ (2010) Nanoparticle, size, shape, and interfacial effects on leakage current density, permittivity, and breakdown strength of metal oxide-polyolefin nanocomposites: experiment and theory. *Chem Mater* 22(4):1567–1578. <https://doi.org/10.1021/cm902852h>
53. Luo X, Yang G, Schubert DW (2022) Electrically conductive polymer composite containing hybrid graphene nanoplatelets and carbon nanotubes: synergistic effect and tunable conductivity anisotropy. *Adv Compos Hybrid Mater* 5(1):250–262. <https://doi.org/10.1007/s42114-021-00332-y>
54. Wang Y, Wang P, Du Z, Liu C, Shen C, Wang Y (2022) Electromagnetic interference shielding enhancement of poly (lactic acid)-based carbonaceous nanocomposites by poly (ethylene oxide)-assisted segregated structure: a comparative study of carbon nanotubes and graphene nanoplatelets. *Adv Compos Hybrid Mater* 5(1):209–219. <https://doi.org/10.1007/s42114-021-00320-2>

**Publisher's Note** Springer Nature remains neutral with regard to jurisdictional claims in published maps and institutional affiliations.